Conformational flexibility of RNA polymerase III during transcriptional elongation

THE EMBO JOURNAL

EMBO J. 2010 November 17; 29(22): 3762–3772. PMCID: PMC2989110
Published online 2010 October 22. doi: 10.1038/emboj.2010.266

Conformational flexibility of RNA polymerase III during transcriptional elongation

Carlos Fernández-Tornero,[1,2,*] Bettina Böttcher,[a,1,3,*] Umar Jan Rashid,[1] Ulrich Steuerwald,[1] Beate Flörchinger,[1] Damien P Devos,[1] Doris Lindner,[1] and Christoph W Müller[b,1]

[1]European Molecular Biology Laboratory, Structural and Computational Biology Unit, Heidelberg, Germany
[2]Chemical and Physical Biology Department, Centro de Investigaciones Biológicas-CSIC, Madrid, Spain
[3]Institute of Structural & Molecular Biology, School of Biological Sciences, The University of Edinburgh, Edinburgh, UK
[a]Institute of Structural and Molecular Biology, School of Biological Sciences, The University of Edinburgh, King's Buildings, Mayfield Road, Edinburgh EH9 3JR, UK. Tel.:+ 44 131 6505 699; Fax: + 44 131 650 8650; E-mail: bettina.boettcher@ed.ac.uk
[b]Structural and Computational Biology Unit, European Molecular Biology Laboratory, Meyerhofstrasse 1, Heidelberg 69117, Germany. Tel.: +06 221 387 8320; Fax: +06 221 387 519; E-mail: cmueller@embl.de
[*]These authors contributed equally to this work

Received August 2, 2010; Accepted September 27, 2010.

Abstract

RNA polymerase (Pol) III is responsible for the transcription of genes encoding small RNAs, including tRNA, 5S rRNA and U6 RNA. Here, we report the electron cryomicroscopy structures of yeast Pol III at 9.9 Å resolution and its elongation complex at 16.5 Å resolution. Particle sub-classification reveals prominent EM densities for the two Pol III-specific subcomplexes, C31/C82/C34 and C37/C53, that can be interpreted using homology models. While the winged-helix-containing C31/C82/C34 subcomplex initiates transcription from one side of the DNA-binding cleft, the C37/C53 subcomplex accesses the transcription bubble from the opposite side of this cleft. The transcribing Pol III enzyme structure not only shows the complete incoming DNA duplex, but also reveals the exit path of newly synthesized RNA. During transcriptional elongation, the Pol III-specific subcomplexes tightly enclose the incoming DNA duplex, which likely increases processivity and provides structural insights into the conformational switch between Pol III-mediated initiation and elongation.

Introduction

RNA polymerase (Pol) III synthesizes a set of small, non-translated RNAs that have important functions in the regulation of gene expression (Dieci et al, 2007). They comprise all tRNAs, as well as 5S rRNA, U6 RNA (implicated in pre-mRNA splicing), 7SL RNA (constituting the signal recognition particle scaffold), the RNA components of RNase P and mitochondrial RNA processing enzyme and the rRNA-methylating snR52. Pol III also transcribes so-called BC200 RNA, whose levels appear to be elevated in affected areas of brains in Alzheimer patients (Mus et al, 2007). Moreover, syntheses of Epstein–Barr virus and several adenovirus RNAs are also mediated by Pol III (Pruzan and Flint, 1995; Takada, 2001).

Pol III is a multi-protein assembly constituted by 17 subunits with an overall mass of 0.7 MDa. Pol III is the largest among the three eukaryotic RNA Pols that all share a horseshoe-shaped core consisting of 10 subunits. Five of these subunits are common between Pol I, II and III, while the other subunits show significant similarity (19–36% identical residues). Attached to the core, two more subunits constitute a prominent stalk that is important for transcription initiation in all eukaryotic Pols (Cramer et al, 2008). Whereas Pol II has no additional subunits, Pol I contains two additional polypeptides that form a heterodimer distantly related to transcription factor (TF) IIF, which participates in Pol II-mediated transcriptional initiation (Kuhn et al, 2007). Pol III contains five specific subunits that are known to form two subcomplexes: the C37/C53 heterodimer, the structural counterpart of TFIIF (Cramer et al, 2008), and the C31/C82/C34 heterotrimer related to TFIIE in Pol II-mediated transcription (Carter and

Drouin, 2010).

Saccharomyces cerevisiae subunits C82, C34 and C31, and also their human homologues, constitute a subcomplex involved in the initiation of transcription (Werner et al, 1992; Wang and Roeder, 1997). A C-terminal truncation of subunit C31 compromises Pol III for initiation, and is suppressed by overexpression of the largest Pol III subunit C160, suggesting a direct interaction (Thuillier et al, 1995). Subunit C34 interacts directly with the Brf1 subunit of the Pol III-specific TFIIIB, and mutations that map to C34 are defective in Pol III recruitment to the pre-initiation complex (PIC) and in open complex formation (Brun et al, 1997). Consistent with a direct interaction of Brf1 and C34, protein-DNA cross-linking experiments localized subunit C34 furthest upstream on promoter DNA in initiation complexes (Bartholomew et al, 1993).

Subunits C53 and C37 form a stable heterodimer and have a function in the recognition of the transcription terminator, which in Pol III is formed by a stretch of five thymine bases (Landrieux et al, 2006). A recent report has shown that these subunits are also involved in transcription initiation and elongation through DNA interactions that occur in the DNA-binding cleft (Kassavetis et al, 2010). C53 is known to contact DNA near the downstream end of the transcription complex, whereas C37 can be cross-linked to the upstream non-template strand during elongation (Tate et al, 1998). Deleting the 27 C-terminal residues in subunit C37 results in the loss of subunit C53 and also C11, a core subunit involved in RNA cleavage when Pol III becomes stalled at certain DNA positions (Chedin et al, 1998). Equivalently, substitution of C11 with the *Schizosaccharomyces pombe* orthologue causes the loss of C37 and C53, suggesting that all three subunits are located close to each other in the Pol III complex. The resulting enzyme, known as Pol IIIΔ, shows impaired termination and re-initiation activities (Chedin et al, 1998).

A previous electron cryomicroscopy reconstruction of Pol III allowed us to locate the initiation subcomplex C31/C82/C34 on one side of the DNA-binding cleft, next to the stalk, and subcomplex C37/C53 at the opposite side of the DNA-binding cleft (Fernandez-Tornero et al, 2007). Our current manuscript presents a far more detailed electron cryomicroscopy reconstruction of the Pol III enzyme at sub-nanometer resolution. Sub-classification of particles combined with homology modelling yields a detailed description of the structure and dynamics of the Pol III-specific subcomplexes C31/C82/C34 and C37/C53. Comparison with the Pol III elongation complex determined at 16.5 Å resolution reveals the incoming DNA duplex and for the first time allows following the newly synthesised, exiting RNA. In addition, we observe coordinated conformational changes of the Pol III-specific subcomplexes that completely enclose the incoming DNA complex, thereby providing insights into Pol III transcriptional initiation and processivity.

Results and discussion

Electron cryomicroscopy structure of Pol III at 9.9 Å resolution

We purified the complete Pol III complex containing all 17 subunits from an *S. cerevisiae* strain harbouring a tandem-affinity purification (TAP) tag on subunit C128, following established protocols (Fernandez-Tornero et al, 2007). To further improve sample homogeneity, the final size exclusion chromatographic step was substituted by anion-exchange chromatography, and only the central fractions of the resulting peak were used for the subsequent structure determination (Materials and methods). The sample was monodisperse as observed on a highly defocused electron cryomicroscopy field (Figure 1A), allowing reproducible collection of data under native conditions. A first reconstruction was calculated using all 98 649 particles in the data set and the reported, model-unbiased Pol III structure as starting seed (EMD-1322). The resulting EM map showed high variance at regions previously identified as those corresponding to Pol III-specific subunits. This is coherent with native mass spectrometry data, in which we observed some sub-stoichiometry for the C37/C53 subcomplex, as well as the labile attachment of subunit C34 to the Pol III enzyme (unpublished results). Two-dimensional sub-classification of particles with certain orientations followed by three-dimensional maximum-likelihood sorting (Scheres et al, 2008) of the two-dimensional class averages were used to sort out the different populations in the data set (Supplementary data). Initial sorting by sub-classification and maximum-likelihood methods was followed by further refinement using projection matching and supervised classification. The three resulting volumes share the same core, but two of them, representing one-fourth

of the particles each, show either no density for Pol III-specific subcomplexes (Supplementary Figure S1, volume 1) or only a fraction of them (volume 4). The final electron cryomicroscopy reconstruction, calculated from 47 395 particles, shows a resolution of 9.9 Å and is well defined in all regions (Figure 1B–E). The overall Pol III architecture resembles the other two eukaryotic RNA Pols (De Carlo et al, 2003; Armache et al, 2005; Kuhn et al, 2007), allowing the direct recognition of previously described structural features (Figure 1E).

Structural features of the Pol III core and stalk

To precisely describe the Pol III core, we fitted the available crystal structures of the Pol II core with its clamp element in an open (PDB code 1I50; Cramer et al, 2001) and closed conformation (PDB code 1WCM without stalk; Armache et al, 2005) into the EM reconstruction using program Situs (Wriggers, 2010). Correlation coefficients (0.669 versus 0.674) and visual inspection (Figure 2A) showed the high quality of the fit and confirmed that the Pol III core adopts a closed conformation. Moreover, when the EM map was sharpened with a temperature factor of −400 $Å^2$ (Bottcher et al, 1997; Rosenthal and Henderson, 2003), we were able to visualize isolated α-helices on the surface of the Pol III core at the expected positions (Figure 2B).

The five core subunits common to Pol I, II and III perfectly fit the EM density on the surface of the enzyme at the expected positions (Figure 2A and C), further confirming the quality of our reconstruction and the overall fit of the Pol II core (Figure 2B). For the other five core subunits, most regions fit the map equally well including the clamp and the DNA-binding cleft (Figure 2D). This is remarkable, because in the electron cryomicroscopy structures of both, Pol I and II, the cleft is not as clearly observed or the clamp appears collapsed against the lobe element on the other side of the cleft (Craighead et al, 2002; Kuhn et al, 2007). However, in the current Pol III structure, the clamp adopts exactly the same conformation as in the crystal structure of the complete 12-subunit Pol II (Armache et al, 2005) resulting in identical dimensions for the DNA-binding cleft in depth (60 Å) and width (30 Å). In contrast, the Pol III cleft is slightly longer (100 Å instead of 85 Å), because of the presence of the Pol III-specific subunits (see below).

In our reconstruction, several regions significantly deviate with respect to Pol II (Figure 2A). Compared with Pol II, the foot is 26 residues shorter in Pol III, probably explaining why the crystal structure sticks out of the EM density in this region (Figure 2D, left panel). Besides, we observe additional density between the foot and subunit Rpb8 (dotted line in Figure 2D, left panel), suggesting that in the case of Pol III, these two elements interact. Subunit Rpb9 is the structural homologue of Pol III subunit C11. However, while strong similarity can be observed between their N-terminal domains, the C-terminal domain of C11 shows higher similarity to the C-terminal zinc ribbon of TFIIS, possibly explaining the role of C11 in the intrinsic RNA cleavage activity of Pol III (Chedin et al, 1998). Coherent with this finding, the N-terminal domain of Rpb9 perfectly fits into our EM density, while its C-terminal domain and the connecting linker completely protrude from it (Figure 2D, middle panel). No additional density in the vicinity of the N-terminal domain can account for the C11 C-terminal domain, suggesting that it is highly mobile. Smaller differences between Pol II and III are also well reflected by our map, which include the well-defined protrusion that connects with the lobe in subunit C128 (Figure 2D, right panels, IN-2). However, the additional piece of density at the protrusion cannot be solely explained by additional residues, and may, therefore, also harbour part of the Pol III-specific subcomplexes (see below).

The Pol III reconstruction shows clear density for the stalk composed by subunits C17 and C25 homologous to subunits Rpb4 and Rpb7 in Pol II, respectively. When the crystal structure of the complete 12-subunit Pol II (PDB code 1WCM; Armache et al, 2005) is fitted into our reconstruction, the stalk no longer matches the density and appears slightly bent towards the clamp element (Figure 2E, left panel). We, therefore, fitted the stalk independent from the 10-subunit core as a rigid body into our EM reconstruction using the program Chimera (Pettersen et al, 2004). Fitting the resulting 12-subunit structure using program Situs (Wriggers, 2010) increased the correlation coefficient from 0.714 (initially obtained with the 1WCM structure) to 0.727. Interestingly, the re-adjusted stalk nicely superimposes with the original 12-subunit structure at the tip domain, where it interacts with the Pol core, while the remainder of the stalk rotates by approximately 20° away from the clamp element (Figure 2E, middle and right panel). Our results suggest that the stalk undergoes rotational movements using the tip domain

as a pivot point.

Overall structure of the Pol III-specific subcomplexes

The most striking feature in our reconstruction is the presence of two large density regions that are not occupied by the crystal structure of Pol II (Figures 2A and 3A). Both densities are larger and more continuous compared with our previous reconstruction (Fernandez-Tornero et al, 2007), in which they had been assigned to Pol III-specific subunits. Sub-classification strategies allowed us to exclude particles heterogeneous in these regions, representing about half of the data set (see Supplementary data for details). In particular, 25% of the particles lack both subcomplexes, while 26% show poor density for the C31/C82/C34 subcomplex (Supplementary Figure S1, volumes 1 and 4, respectively). While the Pol III core is well defined in our 9.9 Å resolution map, we observe features radially extending from it (Figure 1E), indicating a greater variability and mobility of these regions. This suggests that the extensions to the core, that is the stalk and Pol III-specific subcomplexes, are probably resolved at slightly lower resolution than the particle core. Our description of these regions will, therefore, refer to an unfiltered map at 11.5 Å resolution resulting from the sub-classification procedure (Supplementary data).

The largest additional density is located between the stalk and the clamp elements (Figure 3A, orange). Whereas it is predominantly attached to the clamp, it also forms two elongated connections with the stalk. Using antibody labelling, we had showed that this density harbours the C31/C82/C34 heterotrimer (Fernandez-Tornero et al, 2007). In the current reconstruction, the corresponding volume is more extended and comprises 157 000 $Å^3$, which represents a molecular mass of 124 kDa considering a protein density of 1.37 g/cm^3 (Harpaz et al, 1994). Given that certain regions of these subunits are predicted unstructured, this is in good agreement with the total mass of the heterotrimer (138 kDa). One of the two elongated stalk connections points towards the core-distant part of the OB domain in subunit C25, and may also contact C17 (Figure 3A, connection 1). The other density connects a Pol III-specific insertion in subunit C25 (residues 160–190) with the 'clamp core' of subunit C160, precisely in which two Zn atoms are present in the Pol II structure (Figure 3A, connection 2). Consistent with the observed EM density, the C31/C82/C34 subcomplex is thought to contact the Pol III core at this region (Werner et al, 1992). As subunit C31 has been proposed to interact with both, the clamp element of the core subunit C160 (Thuillier et al, 1995) and the stalk subunit C17 (Ferri et al, 2000), we hypothesize that C31 indeed mediates this connection.

The second largest additional piece of density is located next to the lobe element of subunit C128 on the opposite side of the DNA-binding cleft (Figure 3A, blue). Apart from the major lobe interaction, this density also contacts the N-terminal domain of subunit C11, equivalent to the N-terminal moiety of Rpb9 (see above). Antibody labelling experiments show that this density corresponds to the C37/C53 heterodimer (Supplementary Figure S2). Sequence analysis indicates that subunits C37 and C53 are the counterpart of subunits Tfg1 and Tfg2 from TFIIF (Cramer et al, 2008), which interact through their dimerization domains to produce a flattened β-barrel. Two reports have located the dimerization domain of TFIIF next to the Pol II lobe element (Chen et al, 2010; Eichner et al, 2010), coherent with the additional density that we observe in Pol III. A similar position has also been proposed for the homologous Pol I heterodimer A49/A34.5 (Kuhn et al, 2007). In our Pol III reconstruction, the volume of this density is 78 000 A^3, which corresponds to 69 kDa and is in good agreement with the total mass of the heterodimer (79 kDa) considering that it contains disordered regions. At lower threshold, we see a fuzzy extension at the tip of this additional density (Figure 3A), which probably represents part of the unstructured regions.

Fitting of the homology model of the C37/C53 dimerization domains into the Pol III structure

The dimerization domains of the C37/C53 subcomplex show sequence similarities to the equivalent regions in TFIIF subunits Tfg1/Tfg2 (Rap74/Rap30 in humans). The crystal structure of the human TFIIF dimerization domains shows that both subunits share the same fold (comprising seven β-strands) and complement each other to form a triple β-barrel (Gaiser et al, 2000). Using hidden Markov model (HMM) approaches, we identified conserved domains in the C53 and C37 subunits (Figure 3B). The C-terminal domain of subunit C53 (residues 300–422) corresponds to the dimerization domain of Rap30, but contains a large insertion between strands 1 and 2 in the β-barrel fold. Similarly, the central region in C37 (residues 70–180) corresponds to the dimerization domain of Rap74 (Figure 3B). Consistent with

these predictions, we were able to co-express and purify the C37/C53 dimerization domains in bacteria. The complex of the C37 and C53 dimerization domains is monodisperse, elutes as a single peak at the expected volume in size exclusion chromatography and contains both domains in stoichiometric amounts (Figure 3C).

Based on our HMM results, we used the program Modeller (Sali and Blundell, 1993) to build a homology model of the C37/C53 dimerization domains (Supplementary Figure S3). Manual fitting readily showed that the C37/C53 triple β-barrel (lacking Pol III-specific insertions) fits well into the volume of the second largest piece of additional density in the EM reconstruction. In order to determine the proper orientation of the triple β-barrel with respect to the Pol III core, we used published distance constraints corresponding to the interaction between pairs of residues in the Pol II lobe element and the yeast TFIIF subunits (Chen et al, 2007, 2010; Eichner et al, 2010). The resulting fit respects most of the described interactions and suggests how the C37/C53 subcomplex is positioned on the Pol core (Figure 3D). The solid, well-defined density for this domain suggests that the dimerization moiety is probably the major anchoring point of this subcomplex on the Pol III core, while most of the remaining regions are presumably flexible.

Fitting of the winged-helix domains present in C31/C82/C34 into the Pol III structure

It has been recently suggested that the C31/C82/C34 heterotrimer is evolutionary related to TFIIE, composed of subunits Tfa1 and Tfa2 (Carter and Drouin, 2010). Although the highest similarity was found between a winged-helix (WH) domain in Tfa1 and two regions in subunit C82 (residues 48–130 and 489–596), an additional WH domain is present in this subunit between residues 151 and 214 (Figure 3B). The similarity between C34 and Tfa1 is less pronounced, but secondary structure analysis suggests the presence of three WH domains in tandem (Figure 3B). The structure of each of the two N-terminal WH domains in C34 has been determined by NMR (PDB codes 2DK8 and 2DK5, respectively). The prediction for the C-terminal WH domain is weaker and it contains a disordered loop insertion (residues 190–212; Supplementary Figure S4). The last 47 C-terminal residues in C34 contain a stretch of acidic residues and, apart from a β-hairpin, are predicted to be intrinsically unfolded. In spite of some helices predicted for C31 (not shown), no relevant structural similarities to TFIIE can be detected. The evolutionary relationship between TFIIE and the C31/C82/C34 heterotrimer is further supported by their similar location relative to their respective RNA Pol cores. TFIIE has been positioned on top of the clamp element on the largest Pol II subunit (Chen et al, 2007) corresponding to the position of the major additional density in our Pol III reconstruction.

The presence of at least six WH domains, a well-known DNA interaction domain, in the C31/C82/C34 heterotrimer is coherent with its role in the initiation of transcription (Werner et al, 1992; Wang and Roeder, 1997). Both subunits, C34 and C82, have been cross-linked to DNA in PICs (Bartholomew et al, 1993; Tate et al, 1998). Based on these results, we have fitted individual WH domains in our major additional EM density. Although the large size of this density makes the unambiguous assignment to specific domains difficult, several rounded features of appropriate size are apparent next to the DNA-binding cleft that could harbour globular WH domains. Three globular densities proximal to the cleft are hypothesized to correspond to the C34 subunit (Figure 3D), which presents the most extensive interaction with DNA (Bartholomew et al, 1993). Moreover, the suggested C34 position is consistent with our native mass spectrometry results that place this protein in the most peripheral location, whereas C82 and C31, which strongly interact, establish intimate contacts with the Pol core (data not shown). Furthermore, subunit C34 has been shown to participate in promoter opening, a process that, contrary to Pol II, does not involve energy uptake (Kassavetis et al, 1992; Brun et al, 1997). Interestingly, a recent report has shown that certain WH domains are able to open the DNA without the need of additional energy, by inserting the C-terminal β-hairpin between the 5′ and 3′ DNA strands (Kitano et al, 2010). In this case, the recognition helix in the WH domain does not contact the DNA, while instead positively charged residues of the β-hairpin mediate the DNA interactions. A similar mechanism may be used by subunit C34, although a structural confirmation of this hypothesis is required (Supplementary Figure S4).

Electron cryomicroscopy structure of a Pol III elongation complex

In order to understand the structural rearrangements that occur during the Pol III elongation process,

the Pol III enzyme was bound to a synthesized DNA/RNA bubble consisting of a 41-mer DNA duplex with a central 11 nucleotide mismatch and a 20-mer RNA with eight nucleotides complementary to the mismatch region of the DNA template strand. Purified Pol III was saturated with a five-fold molar excess of the transcription bubble that after incubation was removed by size exclusion chromatography yielding a homogeneous elongation complex (see Material and methods). The structure of the complex was analysed using electron cryomicroscopy. In total, 22 000 particles were picked and processed using supervised classification (Supplementary Figure S5). Approximately, two-thirds of the particles fell into classes with prominent density for the Pol III-specific subcomplexes C31/C82/C34 and C37/C53. Of these particles, roughly 75% showed additional density in the DNA-binding cleft, resulting in a 3D reconstruction of the Pol III elongation complex at 16.5 Å resolution. When compared with the structure of the empty Pol III using difference mapping, a large continuous positive difference density is observed along the DNA-binding cleft and beyond (Figure 4A and inset). We attribute this major density to the transcription bubble. This is further supported by the fit of the Pol II elongation complex crystal structure (Kettenberger et al, 2004), which places the transcription bubble inside the large positive difference density and confirms that it occupies the same position in Pol II and Pol III (Figure 4A, insets). However, in contrast with the Pol II elongation complex crystal structure only showing electron density for the downstream DNA until position +9, the entire designed downstream DNA until base pair +16 appears to be resolved inside the binding cleft of our Pol III elongation complex electron cryomicroscopy structure. Moreover, the large positive density shows a continuous extension that runs from the DNA/RNA heteroduplex to the stalk (Figure 4A), just above the saddle element (formed by subunits C160 and C128), a region that has been identified as the RNA exit path in Pol II (Andrecka et al, 2008). Modelling an extended RNA comprising 10 additional nucleotides, present in our synthesized bubble, exactly fits the length of the continuous density (Supplementary Figure S6) and reaches the external part of the tip domain in the stalk (Figures 2E and 4A), consistent with the RNA-binding activity of the Pol III stalk observed *in vitro* (Jasiak et al, 2006). We, therefore, conclude that the large positive density reveals the complete exit path for the newly synthesized RNA on the transcribing enzyme. A small piece of density, poorly connected to the density of newly synthesized RNA is present next to the protrusion and may represent part of the upstream DNA duplex (Figure 4B). No particular density could be assigned to the non-coding single DNA strand, probably because it is still very flexible in solution in spite of a described interaction with subunit C37 (Tate et al, 1998).

Apart from the major piece of positive density corresponding to the transcription bubble, the structure of Pol III elongation complex presents several differences with respect to the apo form of the enzyme, principally in the surroundings of the most downstream DNA duplex. As they appear as pairs of negative and positive densities in the difference map (Figure 4B), they are likely to reflect conformational changes occurring in the transition from transcriptional initiation to elongation. One important change occurs for the C31/C82/C34 heterotrimer, which essentially moves away from the stalk towards the DNA-binding site. Concomitant with this movement, the stalk rotates in the opposite direction leading to a weaker connection with the heterotrimer, whereas subunit Rpb5 approaches C31/C82/C34 (Figure 4A). The density corresponding to the C37/C53 dimerization domains remains practically identical compared with the empty form of Pol III, confirming that the triple β-barrel does not occupy the DNA-binding cleft. In addition, a new piece of density connects the dimerization domains with downstream DNA (Figure 4B). We speculate that this density corresponds to disordered regions in C53 that become ordered when the transcription bubble has formed, because this subunit has been shown to bind downstream DNA (Tate et al, 1998). Moreover, the additional density on top of the protrusion element (Figure 2D), that may contain part of the C37/C53 subcomplex or the upstream DNA duplex (see above), bends towards the DNA-binding cleft. The observed densities are consistent with a recent report showing that part of the C37/C53 subcomplex lies inside the DNA-binding cleft, explaining its role in transcription initiation, elongation (Kassavetis et al, 2010) and termination (Landrieux et al, 2006). Another important difference between Pol III and its elongation complex appears at the top of the cleft entrance. Whereas in the apo form of Pol III the two densities, each corresponding to one of the Pol III-specific subcomplexes, barely contact each other (arrowed star in Figure 3A), this contact becomes more prominent in the elongation complex, suggesting that both subcomplexes move towards each other and enclose the incoming DNA (Figure 4, compare also the movies showing the changes in the Supplementary data).

Model for Pol III closed and open PICs

In the last step of the Pol III recruitment process, TFIIIB, a heterotrimer composed of subunits TBP, Brf1 and Bdp1, brings the enzyme to the transcription start site. Brf1 is a large polypeptide with an N-terminal TFIIB-homologous moiety (Figure 5A, green) and a C-terminal Pol III-specific part that contains the conserved Brf1-homology regions I to III (Khoo et al, 1994). To understand the role of Pol III-specific subcomplexes in transcriptional initiation, we have used our 3D reconstruction and available structural data to build models of the Pol III non-transcriptional active, closed and open PICs. Available crystal structures include Brf1-homology region II in complex with TBP and DNA (Juo et al, 2003), TFIIB in complex with Pol II (Kostrewa et al, 2009; Liu et al, 2010) and TFIIB in complex with TBP and DNA (Nikolov et al, 1995).

In the resulting PIC models (Figure 5), the last residue of the Brf1-homology region II (Glu506) lies at a distance of only 25 Å from the density assigned to subcomplex C31/C82/C34. This distance can be easily bridged by the C-terminal tail of subunit C34 and the C-terminal domain of Brf1, in agreement with the reported interaction between Brf1 and C34 (Andrau et al, 1999). The close proximity of both subunits further validates our positioning of C34 in the area that is closest to the DNA-binding cleft. This position is also coherent with DNA cross-linking experiments (Bartholomew et al, 1993; Tate et al, 1998) that locate subunit C34 to the most upstream position of the DNA between positions −5 and −17 in the closed PIC. Our positioning of subunit C34 next to the DNA-binding cleft and of subunit C31 next to the clamp core and stalk elements implies that subunit C82 occupies the remaining density. Cross-linking experiments (Tate et al, 1998) and the presence of WH domains in this subunit suggest a role in DNA binding for this subunit. We propose that some of the WH domains in C82 are positioned between C34 and subunit Rpb5, where they are able to interact with DNA. Interestingly, an equivalent position is occupied by the WH-containing subunit Rpo13 in archaeal RNA Pol (Korkhin et al, 2009). Whether these domains are functionally similar will require further investigation.

The two major additional density features, corresponding to subcomplexes C31/C82/C34 and C37/C53, almost contact each other at the top of the cleft entrance (Figures 1E and 3A). Promoter melting in Pol III requires subunit C34 in coordination with TFIIIB subunits Brf1 and Bdp1 (Kassavetis et al, 1992), and involves conformational rearrangements that allow the melted DNA to fall inside its binding cleft. Given the conformational changes of C31/C82/C34 that we have observed, this subcomplex presumably undergoes a major change in the transition from closed to open PIC. In the elongation complex, the contact between subcomplexes C31/C82/C34 and C37/C53 at the cleft entrance becomes much more prominent (Figure 4). This is likely to hinder the enzyme from falling off the DNA and, therefore, enhances its processivity. Moreover, Pol III directs several rounds of transcription on the same gene once attached to DNA, an event known as facilitated re-initiation (Dieci and Sentenac, 1996) in which subunits C37 and C53, together with C11, are involved (Landrieux et al, 2006). The enclosure of downstream DNA likely decreases the speed at which the enzyme detaches from the template once the transcription terminator is reached, thereby providing time that may allow facilitated re-initiation to occur more easily.

Materials and methods

Pol III isolation and elongation complex preparation

S. cerevisiae Pol III was isolated from a yeast strain modified to express endogenous C128 fused with a C-terminal TAP-tag using previously described procedures (Fernandez-Tornero et al, 2007). The final size exclusion chromatography was substituted by anion-exchange chromatography (MonoQ 10/10, GE-Healthcare) as described (Huet et al, 1996). The Pol III enzyme elutes as a single peak with a maximum corresponding to a conductivity of 60 mS/cm. An artificial transcription bubble was prepared as previously described (Kettenberger et al, 2004) and was added in five molar excess to purified Pol III. Unbound transcription bubble was subsequently removed using size exclusion chromatography on a Superose 6 column (GE-Healthcare) in 10 mM Tris pH 7.5, 100 mM ammonium sulphate, 10 mM DTT.

Recombinant protein expression and purification

The C37/C53 dimerization domains were co-expressed using vectors pETMCN-His (Romier et al, 2006) encoding for the N-terminally His-tagged C53 dimerization domain (residues 289–422), and pETMCN encoding for the untagged dimerization domain of C37 (residues 68–189). The complex was expressed

for 15 h at 18° in *E. coli* BL21 Star (DE3) cells (Invitrogen). Harvested cells were lysed in 50 mM Tris pH 7.4, 300 mM NaCl, 2 mM β-mercaptoethanol, 15 mM imidazole, cleared by centrifugation for 1 h at 30 000 *g* and subsequently applied to equilibrated Ni-NTA (Qiagen) resin. Proteins were eluted in the same buffer containing 250 mM imidazole and incubated with TEV protease to remove the His-tag. As a final step, the complex was purified by size exclusion chromatography (Superdex 200 10/300, GE-Healthcare) equilibrated in 10 mM Tris pH 7.4, 150 mM NaCl.

Electron cryomicroscopy

Samples were prepared for electron cryomicroscopy as described earlier (Fernandez-Tornero et al, 2007). For empty Pol III, we used homemade holey carbon grids with irregular holes, while for the Pol III elongation complex, lacey carbon film was used to increase the number of particles inside the holes. Frozen grids were stored in liquid nitrogen until use. Grids were transferred at low temperature (< −170°C) to an FEI CM200 FEG electron microscope using a Gatan cryo-transfer holder (Gatan 626). The microscope was operated under low-dose conditions at an accelerating voltage of 200 kV. Micrographs were recorded on Kodak SO 163 film at a nominal magnification of 50 000, and visually inspected for lack of charging and drift. Those of suitable quality were scanned with a Zeiss Scai scanner. For empty Pol III, we scanned 699 micrographs at 7 μm per pixel, corresponding to 1.4 Å at specimen level. For the Pol III elongation complex, 47 micrographs were scanned at 14 μm per pixel corresponding to a pixel size of 2.8 Å at specimen level.

Image processing

The contrast transfer function of the micrographs was determined with program ctffind3 (Mindell and Grigorieff, 2003). Micrographs were retained only if Thon rings in the background-subtracted power spectrum were visible in all directions to at least 1/13 $Å^{-1}$ for empty Pol III and 1/15 $Å^{-1}$ for the Pol III elongation complex. According to these quality criteria, 593 and 39 micrographs of empty Pol III and the Pol III elongation complex, respectively, were used for further processing. Particle images were selected manually with program boxer of the EMAN package (Ludtke et al, 1999). We selected 113 173 particles for empty Pol III and 23 792 particles for the Pol III elongation complex. Further image processing was carried out with Spider (Shaikh et al, 2008) using iterative projection matching and sub-classification. Imagic (van Heel et al, 1996) and three-dimensional maximum-likelihood-classification of Xmipp (Scheres et al, 2008) were used for determining the three-dimensional starting models for further supervised classification. For details, see Supplementary data.

Secondary structure prediction and modelling

Similar proteins were identified using Psi-Blast. Secondary structure elements (α-helices and β-strands) were predicted with the PSI-PRED program (Jones, 1999). HMM were built and compared with a database of PDB-derived HMM using the suite of programmes available in the HHPred package (Soding, 2005). Three-dimensional all-atoms models were built with Modeller (Sali and Blundell, 1993).

Accession numbers

The electron cryomicroscopy maps corresponding to the structures of Pol III and its elongation complex have been deposited at the Electron Microscopy Data Bank (EMDB) under the accession numbers EMD-1802, EMD-1803 and EMD-1804.

Supplementary Material

Supplementary Movie 1:
Supplementary Movie 2:
Supplementary Data:
Review Process File:

Acknowledgments

We are grateful to Óscar Llorca, Estela Pineda-Molina and Sebastian Glatt for critically reading the manuscript. We thank Marielle Bauzan at the Institut de Biologie Structurale et Moleculaire IFR 88 (Marseille) and Emmanuel Poilpré at the Protein Expression and Purification Core Facility, EMBL

Heidelberg for yeast fermentation and the Monoclonal Antibodies Core Facility, EMBL Monterotondo for monoclonal C53 antibodies. The project has been supported by the EU-Grant '3D repertoire', Contract no. LSHG-CT-2005-512028.

Footnotes

The authors declare that they have no conflict of interest.

References

- Andrau JC, Sentenac A, Werner M (1999) Mutagenesis of yeast TFIIIB70 reveals C-terminal residues critical for interaction with TBP and C34. J Mol Biol 288: 511–520. [PubMed: 10329159]
- Andrecka J, Lewis R, Brückner F, Lehmann E, Cramer P, Michaelis J (2008) Single-molecule tracking of mRNA exiting from RNA polymerase II. Proc Natl Acad Sci USA 105: 135–140. [PMCID: PMC2224174] [PubMed: 18162559]
- Armache KJ, Mitterweger S, Meinhart A, Cramer P (2005) Structures of complete RNA polymerase II and its subcomplex, Rpb4/7. J Biol Chem 280: 7131–7134. [PubMed: 15591044]
- Bartholomew B, Durkovich D, Kassavetis GA, Geiduschek EP (1993) Orientation and topography of RNA polymerase III in transcription complexes. Mol Cell Biol 13: 942–952. [PMCID: PMC358978] [PubMed: 8423814]
- Bottcher B, Wynne SA, Crowther RA (1997) Determination of the fold of the core protein of hepatitis B virus by electron cryomicroscopy. Nature 386: 88–91. [PubMed: 9052786]
- Brun I, Sentenac A, Werner M (1997) Dual role of the C34 subunit of RNA polymerase III in transcription initiation. EMBO J 16: 5730–5741. [PMCID: PMC1170204] [PubMed: 9312031]
- Carter R, Drouin G (2010) The increase in the number of subunits in eukaryotic RNA polymerase III relative to RNA polymerase II is due to the permanent recruitment of general transcription factors. Mol Biol Evol 27: 1035–1043. [PubMed: 20026480]
- Chedin S, Riva M, Schultz P, Sentenac A, Carles C (1998) The RNA cleavage activity of RNA polymerase III is mediated by an essential TFIIS-like subunit and is important for transcription termination. Genes Dev 12: 3857–3871. [PMCID: PMC317263] [PubMed: 9869639]
- Chen HT, Warfield L, Hahn S (2007) The positions of TFIIF and TFIIE in the RNA polymerase II transcription preinitiation complex. Nat Struct Mol Biol 14: 696–703. [PMCID: PMC2483787] [PubMed: 17632521]
- Chen ZA, Jawhari A, Fischer L, Buchen C, Tahir S, Kamenski T, Rasmussen M, Lariviere L, Bukowski-Wills JC, Nilges M, Cramer P, Rappsilber J (2010) Architecture of the RNA polymerase II-TFIIF complex revealed by cross-linking and mass spectrometry. EMBO J 29: 717–726. [PMCID: PMC2810376] [PubMed: 20094031]
- Craighead JL, Chang WH, Asturias FJ (2002) Structure of yeast RNA polymerase II in solution: implications for enzyme regulation and interaction with promoter DNA. Structure 10: 1117–1125. [PubMed: 12176389]
- Cramer P, Armache KJ, Baumli S, Benkert S, Brueckner F, Buchen C, Damsma GE, Dengl S, Geiger SR, Jasiak AJ, Jawhari A, Jennebach S, Kamenski T, Kettenberger H, Kuhn CD, Lehmann E, Leike K, Sydow JF, Vannini A (2008) Structure of eukaryotic RNA polymerases. Annu Rev Biophys 37: 337–352. [PubMed: 18573085]
- Cramer P, Bushnell DA, Kornberg RD (2001) Structural basis of transcription: RNA polymerase II at 2.8 angstrom resolution. Science 292: 1863–1876. [PubMed: 11313498]
- De Carlo S, Carles C, Riva M, Schultz P (2003) Cryo-negative staining reveals conformational flexibility within yeast RNA polymerase I. J Mol Biol 329: 891–902. [PubMed: 12798680]
- Dieci G, Fiorino G, Castelnuovo M, Teichmann M, Pagano A (2007) The expanding RNA polymerase III transcriptome. Trends Genet 23: 614–622. [PubMed: 17977614]
- Dieci G, Sentenac A (1996) Facilitated recycling pathway for RNA polymerase III. Cell 84: 245–252. [PubMed: 8565070]
- Eichner J, Chen HT, Warfield L, Hahn S (2010) Position of the general transcription factor TFIIF within the RNA polymerase II transcription preinitiation complex. EMBO J 29: 706–716. [PMCID: PMC2829161] [PubMed: 20033062]
- Fernandez-Tornero C, Bottcher B, Riva M, Carles C, Steuerwald U, Ruigrok RW, Sentenac A,

Muller CW, Schoehn G (2007) Insights into transcription initiation and termination from the electron microscopy structure of yeast RNA polymerase III. Mol Cell 25: 813–823. [PubMed: 17386259]

- Ferri ML, Peyroche G, Siaut M, Lefebvre O, Carles C, Conesa C, Sentenac A (2000) A novel subunit of yeast RNA polymerase III interacts with the TFIIB-related domain of TFIIIB70. Mol Cell Biol 20: 488–495. [PMCID: PMC85110] [PubMed: 10611227]
- Gaiser F, Tan S, Richmond TJ (2000) Novel dimerization fold of RAP30/RAP74 in human TFIIF at 1.7 A resolution. J Mol Biol 302: 1119–1127. [PubMed: 11183778]
- Harpaz Y, Gerstein M, Chothia C (1994) Volume changes on protein folding. Structure 2: 641–649. [PubMed: 7922041]
- Huet J, Manaud N, Dieci G, Peyroche G, Conesa C, Lefebvre O, Ruet A, Riva M, Sentenac A (1996) RNA polymerase III and class III transcription factors from Saccharomyces cerevisiae. Methods Enzymol 273: 249–267. [PubMed: 8791617]
- Jasiak AJ, Armache KJ, Martens B, Jansen RP, Cramer P (2006) Structural biology of RNA polymerase III: subcomplex C17/25 X-ray structure and 11 subunit enzyme model. Mol Cell 23: 71–81. [PubMed: 16818233]
- Jones DT (1999) Protein secondary structure prediction based on position-specific scoring matrices. J Mol Biol 292: 195–202. [PubMed: 10493868]
- Juo ZS, Kassavetis GA, Wang J, Geiduschek EP, Sigler PB (2003) Crystal structure of a transcription factor IIIB core interface ternary complex. Nature 422: 534–539. [PubMed: 12660736]
- Kassavetis GA, Blanco JA, Johnson TE, Geiduschek EP (1992) Formation of open and elongating transcription complexes by RNA polymerase III. J Mol Biol 226: 47–58. [PubMed: 1619662]
- Kassavetis GA, Prakash P, Shim E (2010) The C53/C37 subcomplex of RNA polymerase III lies near the active site and participates in promoter opening. J Biol Chem 285: 2695–2706. [PMCID: PMC2807326] [PubMed: 19940126]
- Kettenberger H, Armache KJ, Cramer P (2004) Complete RNA polymerase II elongation complex structure and its interactions with NTP and TFIIS. Mol Cell 16: 955–965. [PubMed: 15610738]
- Khoo B, Brophy B, Jackson SP (1994) Conserved functional domains of the RNA polymerase III general transcription factor BRF. Genes Dev 8: 2879–2890. [PubMed: 7995525]
- Kitano K, Kim SY, Hakoshima T (2010) Structural basis for DNA strand separation by the unconventional winged-helix domain of RecQ helicase WRN. Structure 18: 177–187. [PubMed: 20159463]
- Korkhin Y, Unligil UM, Littlefield O, Nelson PJ, Stuart DI, Sigler PB, Bell SD, Abrescia NG (2009) Evolution of complex RNA polymerases: the complete archaeal RNA polymerase structure. PLoS Biol 7: e102. [PMCID: PMC2675907] [PubMed: 19419240]
- Kostrewa D, Zeller ME, Armache KJ, Seizl M, Leike K, Thomm M, Cramer P (2009) RNA polymerase II-TFIIB structure and mechanism of transcription initiation. Nature 462: 323–330. [PubMed: 19820686]
- Kuhn CD, Geiger SR, Baumli S, Gartmann M, Gerber J, Jennebach S, Mielke T, Tschochner H, Beckmann R, Cramer P (2007) Functional architecture of RNA polymerase I. Cell 131: 1260–1272. [PubMed: 18160037]
- Landrieux E, Alic N, Ducrot C, Acker J, Riva M, Carles C (2006) A subcomplex of RNA polymerase III subunits involved in transcription termination and reinitiation. EMBO J 25: 118–128. [PMCID: PMC1356358] [PubMed: 16362040]
- Liu X, Bushnell DA, Wang D, Calero G, Kornberg RD (2010) Structure of an RNA polymerase II-TFIIB complex and the transcription initiation mechanism. Science 327: 206–209. [PMCID: PMC2813267] [PubMed: 19965383]
- Ludtke SJ, Baldwin PR, Chiu W (1999) EMAN: semiautomated software for high-resolution single-particle reconstructions. J Struct Biol 128: 82–97. [PubMed: 10600563]
- Mindell JA, Grigorieff N (2003) Accurate determination of local defocus and specimen tilt in electron microscopy. J Struct Biol 142: 334–347. [PubMed: 12781660]
- Mus E, Hof PR, Tiedge H (2007) Dendritic BC200 RNA in aging and in Alzheimer's disease. Proc

Natl Acad Sci USA 104: 10679–10684. [PMCID: PMC1965572] [PubMed: 17553964]
- Nikolov DB, Chen H, Halay ED, Usheva AA, Hisatake K, Lee DK, Roeder RG, Burley SK (1995) Crystal structure of a TFIIB-TBP-TATA-element ternary complex. Nature 377: 119–128. [PubMed: 7675079]
- Pettersen EF, Goddard TD, Huang CC, Couch GS, Greenblatt DM, Meng EC, Ferrin TE (2004) UCSF Chimera—a visualization system for exploratory research and analysis. J Comput Chem 25: 1605–1612. [PubMed: 15264254]
- Pruzan R, Flint SJ (1995) Transcription of adenovirus RNA polymerase III genes. Curr Top Microbiol Immunol 199 (Pt 1): 201–226. [PubMed: 7555055]
- Romier C, Ben Jelloul M, Albeck S, Buchwald G, Busso D, Celie PH, Christodoulou E, De Marco V, van Gerwen S, Knipscheer P, Lebbink JH, Notenboom V, Poterszman A, Rochel N, Cohen SX, Unger T, Sussman JL, Moras D, Sixma TK, Perrakis A (2006) Co-expression of protein complexes in prokaryotic and eukaryotic hosts: experimental procedures, database tracking and case studies. Acta Crystallogr D Biol Crystallogr 62: 1232–1242. [PubMed: 17001100]
- Rosenthal PB, Henderson R (2003) Optimal determination of particle orientation, absolute hand, and contrast loss in single-particle electron cryomicroscopy. J Mol Biol 333: 721–745. [PubMed: 14568533]
- Sali A, Blundell TL (1993) Comparative protein modelling by satisfaction of spatial restraints. J Mol Biol 234: 779–815. [PubMed: 8254673]
- Scheres SH, Nunez-Ramirez R, Sorzano CO, Carazo JM, Marabini R (2008) Image processing for electron microscopy single-particle analysis using XMIPP. Nat Protoc 3: 977–990. [PMCID: PMC2778070] [PubMed: 18536645]
- Shaikh TR, Gao H, Baxter WT, Asturias FJ, Boisset N, Leith A, Frank J (2008) SPIDER image processing for single-particle reconstruction of biological macromolecules from electron micrographs. Nat Protoc 3: 1941–1974. [PMCID: PMC2737740] [PubMed: 19180078]
- Soding J (2005) Protein homology detection by HMM-HMM comparison. Bioinformatics 21: 951–960. [PubMed: 15531603]
- Takada K (2001) Role of Epstein-Barr virus in Burkitt's lymphoma. Curr Top Microbiol Immunol 258: 141–151. [PubMed: 11443859]
- Tate JJ, Persinger J, Bartholomew B (1998) Survey of four different photoreactive moieties for DNA photoaffinity labeling of yeast RNA polymerase III transcription complexes. Nucleic Acids Res 26: 1421–1426. [PMCID: PMC147414] [PubMed: 9490787]
- Thuillier V, Stettler S, Sentenac A, Thuriaux P, Werner M (1995) A mutation in the C31 subunit of Saccharomyces cerevisiae RNA polymerase III affects transcription initiation. EMBO J 14: 351–359. [PMCID: PMC398089] [PubMed: 7835345]
- van Heel M, Harauz G, Orlova EV, Schmidt R, Schatz M (1996) A new generation of the IMAGIC image processing system. J Struct Biol 116: 17–24. [PubMed: 8742718]
- Wang Z, Roeder RG (1997) Three human RNA polymerase III-specific subunits form a subcomplex with a selective function in specific transcription initiation. Genes Dev 11: 1315–1326. [PubMed: 9171375]
- Werner M, Hermann-Le Denmat S, Treich I, Sentenac A, Thuriaux P (1992) Effect of mutations in a zinc-binding domain of yeast RNA polymerase C (III) on enzyme function and subunit association. Mol Cell Biol 12: 1087–1095. [PMCID: PMC369540] [PubMed: 1545791]
- Wriggers W (2010) Using Situs for the integration of multi-resolution structures. Biophys Rev 2: 21–27. [PMCID: PMC2821521] [PubMed: 20174447]

Figures and Tables

Figure 1

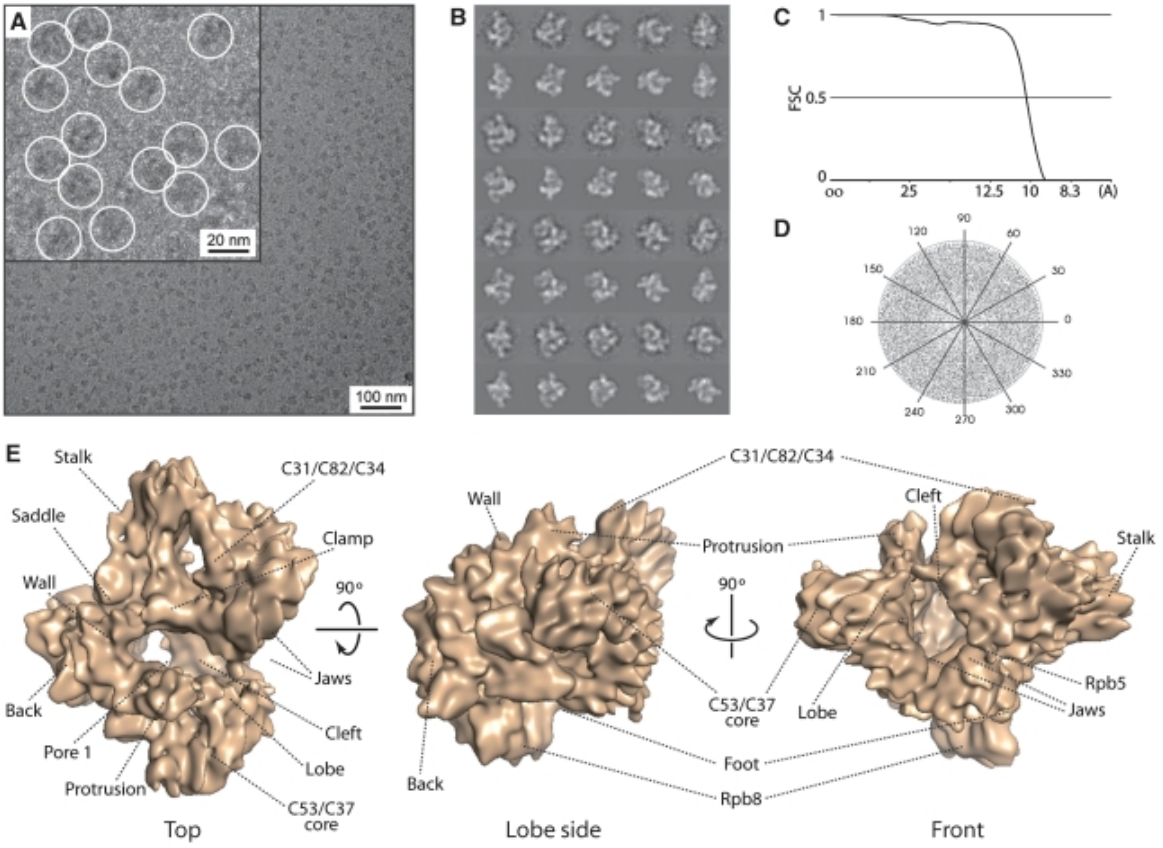

Sub-nanometer structure of yeast Pol III. (**A**) Electron cryomicroscopy field of unstained Pol III particles (circle) in vitrified water. (**B**) Comparison of class averages (odd rows) and model reprojections (even rows) in different orientations. (**C**) Fourier shell correlation (FSC) function curve, showing a resolution of 9.9 Å when a cutoff value of FSC=0.5 is used. (**D**) Distribution of projection angles of the 3D reconstruction showing the approximate number of particles in each orientation. (**E**) Electron cryomicroscopy reconstruction of Pol III. Views and structural regions are named according to the Pol II structure (Cramer et al, 2001).

Figure 2

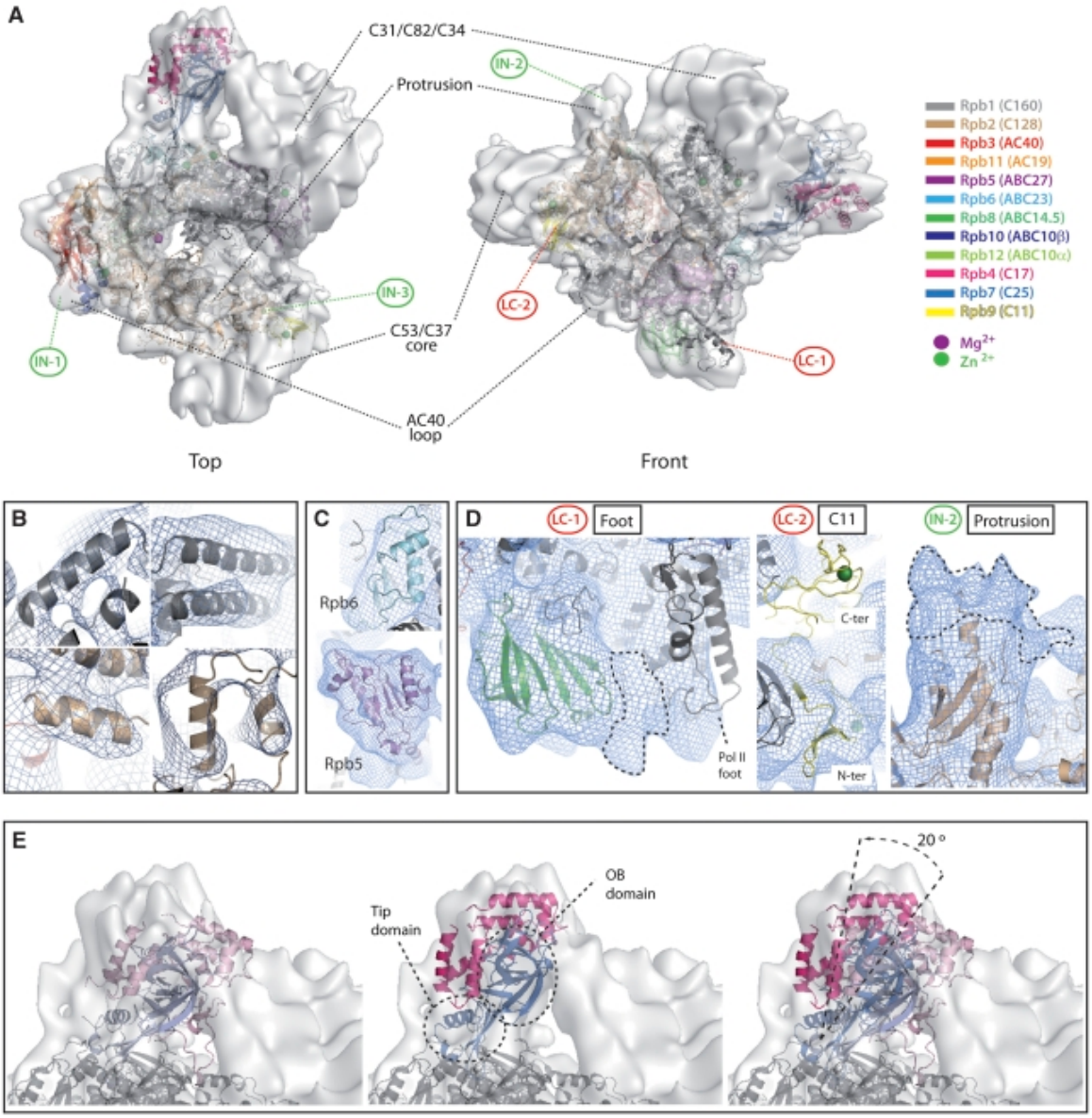

Structural differences between Pol III and II. (**A**) Fitting of the complete 12-subunit Pol II structure shown as ribbon model into the EM density (transparent surface). The fitting was performed in two rigid-body steps, first the 10-subunit core, then the stalk, as explained in the text. The structural elements showing the major differences (LC and IN stand for 'low conservation' and 'insertion') are labelled and numbered (see panel **D** for zoom). Subunit colouring is according to the legend on the right side. (**B**) Examples of regions where the temperature factor-sharpened EM map allows the identification of α-helices. (**C**) Fit of the common subunits Rpb5 and Rpb6 into the Pol III EM reconstruction. (**D**) Detailed views of some of the structural differences between the Pol III EM structure and the Pol II crystal structure. Zn^{2+} ions are depicted as green spheres. (**E**) Close-up view of the Pol III stalk. Left panel: position of the Pol II stalk with the 12-subunit crystal structure (1WCM) superimposed onto the fitted 10 subunits. Pol II subunits Rpb4 and Rpb7 are coloured pink and blue, respectively. Middle panel: independent fitting of the Pol II stalk into the Pol III electron cryomicroscopy reconstruction. The tip and OB domains in subunit Rpb7 (C25 orthologue) are indicated. Right panel: comparison of the Pol II stalk in the left panel with the independently fitted stalk structure.

Figure 3

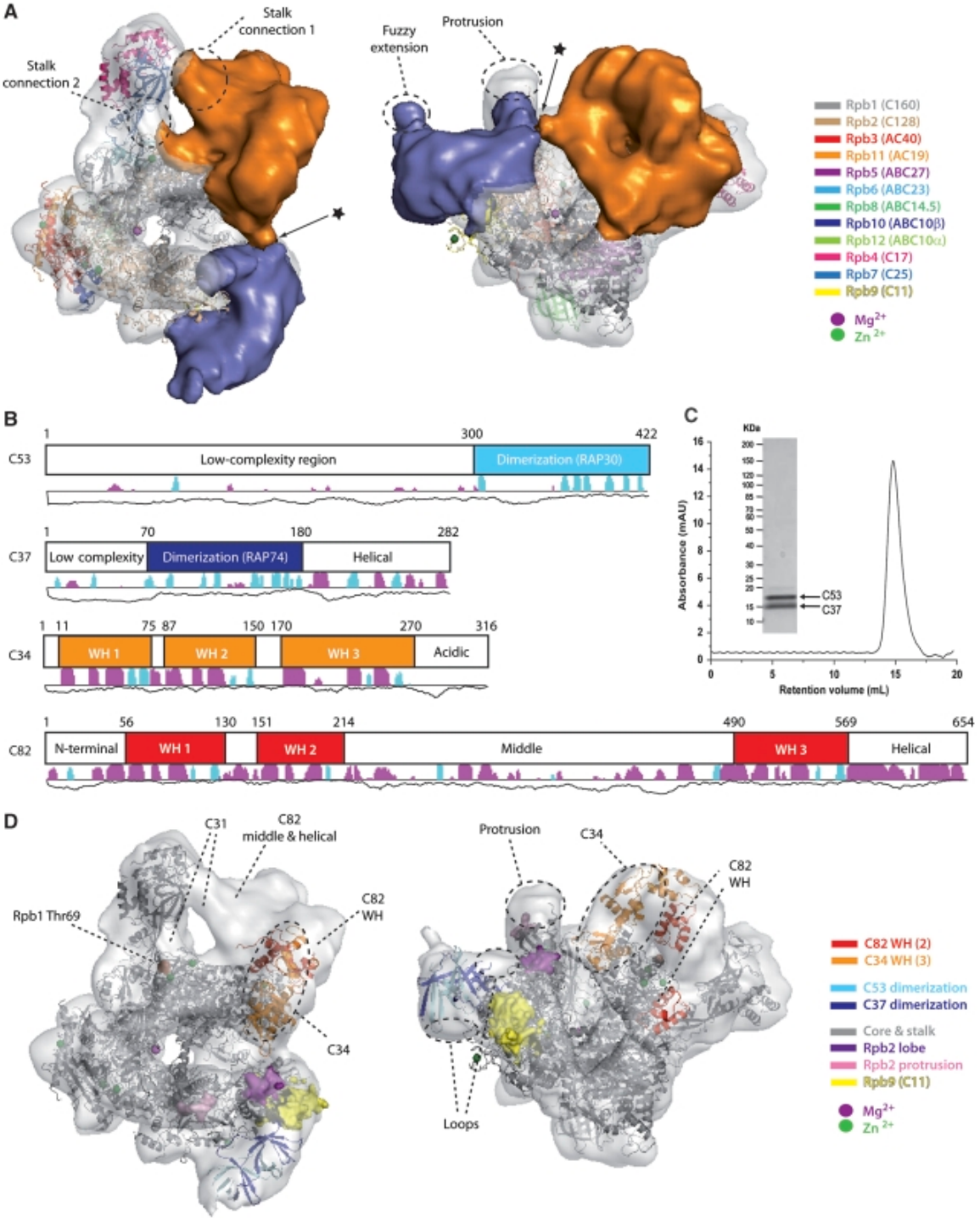

Architecture of the Pol III-specific subcomplexes. (**A**) The additional density on the clamp element next to the stalk (orange) corresponds to the C31/C82/C31 heterotrimer, whereas the additional density next to the lobe element (blue) corresponds to the C37/C53 heterodimer. (**B**) Domain organization of subunits C82, C34, C37 and C53. The probability of a residue to fold into an α-helix or a β-strand is represented by a magenta and light-blue column, respectively. The propensity of a residue to be ordered is indicated below with a continuous black line (top ordered, bottom disorder). (**C**) SDS–PAGE analysis and gel-filtration profile of the purified C37/C53 dimerization domain. The elution volume corresponds to a globular mass of about 30 kDa, in agreement with that of the expressed domain (29 kDa). (**D**) Manual fitting of the C37/C53 dimerization domain and of five out of the six WH domains identified in subunits C82 and C34. The Rpb1 residue Thr69 important for the interaction of the Pol III core with the heterotrimer is shown in orange. The Rpb2 lobe and protrusion elements, identified as the docking region for C37/C53, are shown in magenta and pink, while the N-terminal domain of subunit Rpb9 equivalent to the N-terminal domain of Pol III subunit C11 is depicted in yellow.

Figure 4

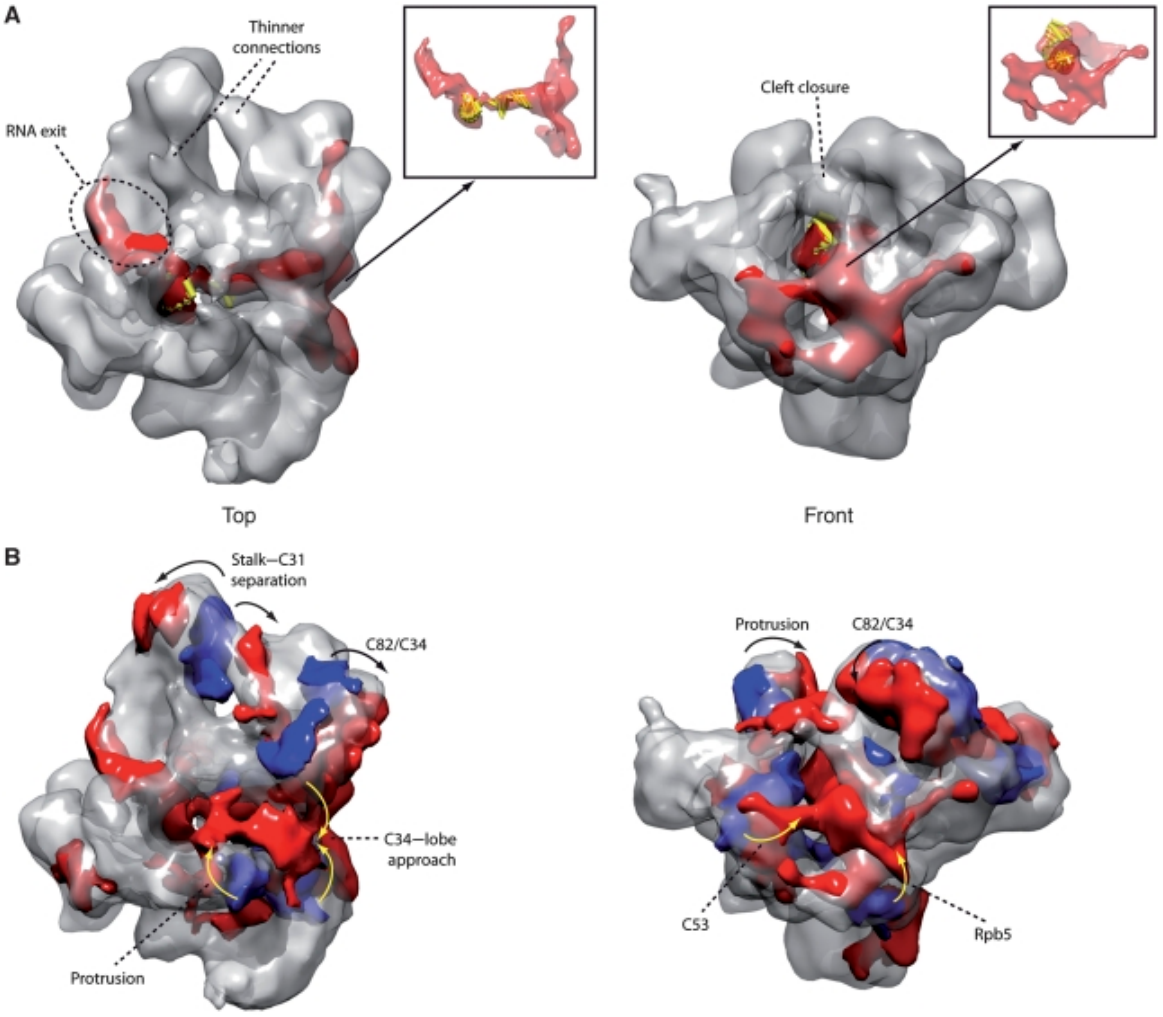

Electron cryomicroscopy structure of the Pol III elongation complex. (**A**) Pol III elongation complex structure at 16.5 Å resolution. The Pol II elongation complex (Kettenberger et al, 2004) has been fitted into the EM density. Only the transcription bubble atomic structure is depicted in yellow. The insets show the largest, continuous segment of positive density in the difference map assigned to the transcription bubble, exiting RNA and the most important rearrangements of the Pol III-specific subcomplexes. (**B**) Difference map between Pol III (white semitransparent density) and its elongation complex with the positive and negative densities shown in red and blue, respectively. The most important structural rearrangements are indicated.

Figure 5

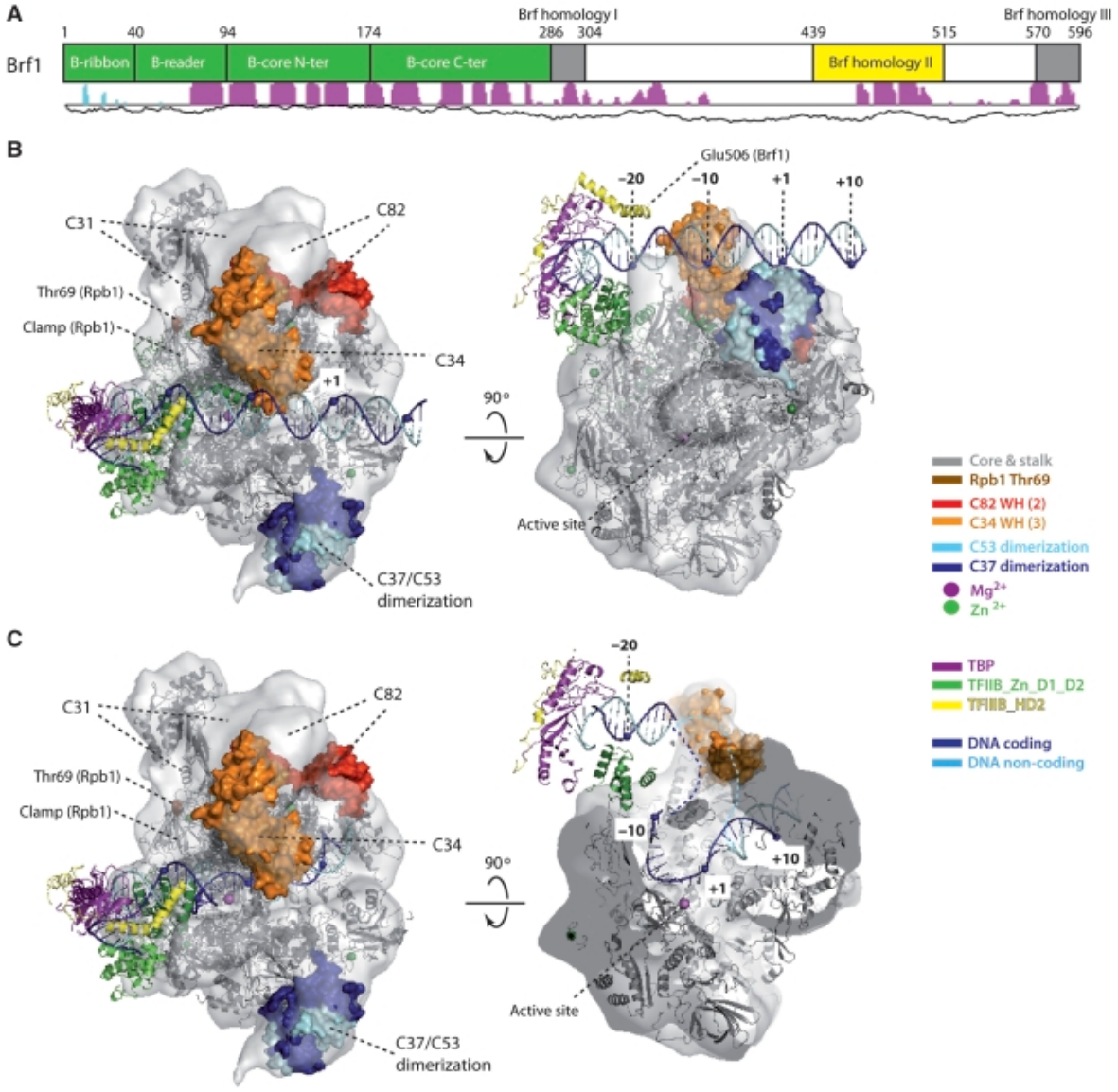

Pre-initiation complex models. (**A**) Domain organization of TFIIIB subunit Brf1. (**B**) Model of the closed PIC obtained by sequential superposition of the Pol II-TFIIB crystal structure (PDB code 3K7A) onto our Pol II core fit, then the TFIIB-TBP-DNA crystal structure (PDB code 1VOL) onto the obtained position of the B-core N-terminal cyclin fold, and finally the crystal structure of the Brf1-homology region II (residues 439–515) in complex with TBP and DNA (PDB code 1NGM) onto our previous positioning of TBP and DNA. An ideal B-form DNA was used to extend from the crystal structure, and the nucleotide positions −20, −10 and +1, +10 are indicated. The left panel orientation corresponds to the top view, rotated about 40° along a vertical axis. (**C**) Model of the open PIC obtained as before but, instead of adding a piece of straight DNA, we superposed the Pol II elongation complex (PDB code 1I6H) onto our Pol II core fit and, after removal of the RNA strand, connected the TATA-bound DNA to the elongating DNA with dashed lines.